Received February 8, 2021, accepted February 15, 2021, date of publication February 23, 2021, date of current version March 4, 2021.

Digital Object Identifier 10.1109/ACCESS.2021.3061473

Multi-Objective Optimization Design of Natural Frequency of Two-Degree-of-Freedom Fast Steering Mirror System

WEIFAN ZHANG[1,2], JING YUAN[1,2], CHANGXIANG YAN[1,3], ZHILIANG GAO[1], AND YOUZHI DONG[1,2]

[1]Changchun Institute of Optics, Fine Mechanics and Physics, Chinese Academy of Sciences, Changchun 130033, China
[2]University of Chinese Academy of Sciences, Beijing 100049, China
[3]Center of Materials Science and Optoelectrics Engineering, University of Chinese Academy of Science, Beijing 100049, China

Corresponding author: Changxiang Yan (yancx@ciomp.ac.cn)

This work was supported in part by the National Key Research and Development Program of China under Grant 2016YFF0103603; in part by the National Natural Science Foundation of China (NSFC) under Grant 61627819, Grant 61727818, Grant 6187030909, and Grant 61875192; and in part by the National Natural Science Foundation of China Youth Fund under Grant 61805235.

ABSTRACT In the design of two-degree-of-freedom (2-DOF) fast steering mirror (FSM) system, in order to improve the control bandwidth of the system, the low-order natural frequency in the working direction should be reduced as much as possible, and the high-order natural frequency in the non-working direction should be increased. In this paper, a deep-cut flexure hinge mirror system was studied. Firstly, the motion direction of the first to third order natural vibration mode of the system was analyzed. Next, the working stiffness in the third vibration mode direction was deduced to solve the problem that the traditional stiffness calculation method is not suitable for the third vibration mode direction. Then, the energy method and the Castigliano's second theorem were used to analyze the working stiffness of the deep-cut flexure hinge. Next, the formula for calculating the relationship between the thickness of the mirror and the moment of inertia in the direction of the vibration mode was derived. Combined with the calculation formula of working stiffness in the vibration mode direction, the formula of the first to third order natural frequencies was derived, and the finite element verification and sensitivity analysis of structural parameters were carried out. Finally, by using NSGA-II, a multi-objective optimization design was carried out on the first to third natural frequencies of the system with hinge structure parameters and reflector thickness as independent variables, and the optimization results were analyzed by theoretical calculation and finite element simulation verification. The results show that the first and second-order natural frequencies of fast steering mirror system are reduced by 7.8% and 7.11%, and the third-order natural frequencies are increased by 139.8%. It proves that the optimized structure is much better than the original structure, and the optimal calculation can effectively increase the control bandwidth of the system

INDEX TERMS Multi-objective optimization, natural frequency, two-degree-of-freedom fast steering mirror, moment of inertia, deep-cut flexure hinge.

I. INTRODUCTION

.Fast steering mirror (FSM) is a mirror device that can precisely control the direction of the beam between the light source and the receiver. It has the characteristics of low power consumption, small size, quick response, and high precision. The FSM system was first used in adaptive optics systems, and is now widely used in precision capture, aiming and tracking, beam stabilization, target pointing, and space laser communication [1]–[9]. For FSM systems, the control bandwidth characterizes the system's ability to track input signals. The higher the value, the faster the system's response speed, which directly reflects the system's accurate and timely tracking ability. In the current situation, the control bandwidth of the large-aperture FSM system generally needs to be improved. Therefore, the FSM system with large-aperture and high control bandwidth is the key field of future FSM system research [10]–[17].

The associate editor coordinating the review of this manuscript and approving it for publication was Guillaume Parent.

Increasing the control bandwidth of the system needs to increase the high-order natural frequency of the system and reduce the low-order natural frequency of the system. Meanwhile, the natural frequency of the system is related to the stiffness and load of the system in the direction of the vibration mode, so we started the research with the working stiffness of the system, the mirror moment of inertia and the calculation formula of natural frequency.

Several scholars have conducted analysis and research on the working stiffness and the calculation formula of the natural frequency in the FSM system. Jinjiang *et al.* [18] analyzed the structure and kinematic stiffness of the FSM support system composed of two free elliptical arc flexure hinges, and conducted experimental verification; Zhiwei *et al.* [19] modeled the FSM system, and discussed the relationship between system mechanical structure and control system; Yafei *et al.* [20] analyzed and calculated the relationship between the stiffness of the fourth-order natural mode of the FSM system and the single flexure hinge, and the relationship between the stiffness of the vibration mode and the natural frequency of the FSM system. The closed-loop bandwidth has been simulated and experimentally analyzed; Ran *et al.* [21] studied the influence of the FSM reaction force on the stability of the system, deduced the corresponding reaction force dynamic equation, and designed a FSM system that can eliminate the influence of the reaction force. The above-mentioned work mainly focuses on the analysis of the stiffness composition and natural frequency of the FSM system, and the design range of stiffness in all directions is obtained through the calculation formula of natural frequency. It matters that little consideration is taken to the influence of the mirror's moment of inertia on the natural frequency of the system, and there is also a lack of quantitative optimization calculations aimed at increasing the system control bandwidth. Therefore, it is necessary to quantitatively analyze the influence of the mirror's moment of inertia on the natural frequency of the system, and perform quantitative multi-objective optimization calculation on the natural frequency of the FSM system with the optimization algorithm.

In response to the above problems, this paper analyzes the natural frequency calculation of the deep-cut flexure hinge FSM system theoretically, and proposes a multi-objective optimization function based on reducing the low-order natural frequency of the system and increasing the high-order natural frequency of the system. First of all, the finite element simulation analysis is conducted on the two-degree-of-freedom (2-DOF) deep-cut flexure hinge FSM system. We obtain the vibration mode of the first three-order natural frequencies, and simplify it in to a spring series-parallel model; aiming at the problem that traditional stiffness analysis is not applicable to the movement direction of the third mode, the relationship between the direction stiffness of the mode-shape and the stiffness of a single flexure hinge is analyzed, and a new theory formula of stiffness in the direction of the third-order mode shape of the FSM is obtained. Then, we firstly use the energy method and Castigliano's second theorem to derive the working stiffness of the deep cut flexure hinge, and simplify it with nonlinear fitting. The simplification solves the problem that the traditional deep cut flexure hinge calculation formula is lengthy. Secondly, we derive the calculation formulas for the moment of inertia of the mirror to the three different rotating shafts under the three different modes of the FSM system, and define the quantitative calculation relationship between the moment of inertia of the mirror and the thickness of the mirror. Thirdly, after that, this paper substitutes the above-derived stiffness calculation formula and the mirror moment of inertia calculation formula into the system's first to third order natural frequency formulas for calculation, and performs finite element simulation verification to prove the accuracy of the first to third order natural frequency calculation formulas. In addition, the Sobol method is used to analyze the sensitivity of the related structural parameters of flexure hinges, mirror thickness and third-order natural frequencies of the system. Finally, we propose a multi-objective optimization function, which uses the NSGA-II algorithm to optimize it and assigns different weights to the third-order natural frequencies of the system. This method can reduce the low-order natural frequency of the system and increase the high-order natural frequency of the system. The optimization results were modeled and verified by finite element simulation. It proves that the optimization calculation effectively reduces the low-order natural frequency of the system and increases the high-order natural frequency of the system. The design results are good, and the theoretical calculation and simulation results are in good agreement. The multi-objective optimization function based on the third-order natural frequency of the system and the derived related theoretical calculation formulas proposed in this paper are of significance for further improving the control bandwidth of the FSM system and optimizing the structure design of the FSM.

II. THEORETICAL FORMULA DERIVATION OF FLEXIBLE SUPPORT SYSTEM FOR FSM

A. EXPERIMENTAL DATASETS DERIVATION OF THE ROTATIONALSTIFFNESS OF FLEXIBLE SUPPORT SYSTEM FOR FSM

The three-dimensional structure models of the fast control mirror and flexible support system discussed in this paper are shown in Fig. 1.

In Fig. 1(a) and Fig. 1(c), the flexible support structure and the isolation plate are connected by bolts; the isolation plate and the reflector are connected by glue. In Fig. 1(b), the coordinate system is o-xyz (o is the rotation center of the flexible support system, and the working direction is rotation around the x and y axes). The structure is composed of 4 flexible hinges with exactly the same structure: the combination of hinges 1 and 3 can realize the deflection of the structure on the x-axis; the combination of hinges 2 and 4 can realize the deflection of the structure on the y-axis. The model of a single deep-cut flexure hinge is shown in Figure 2.

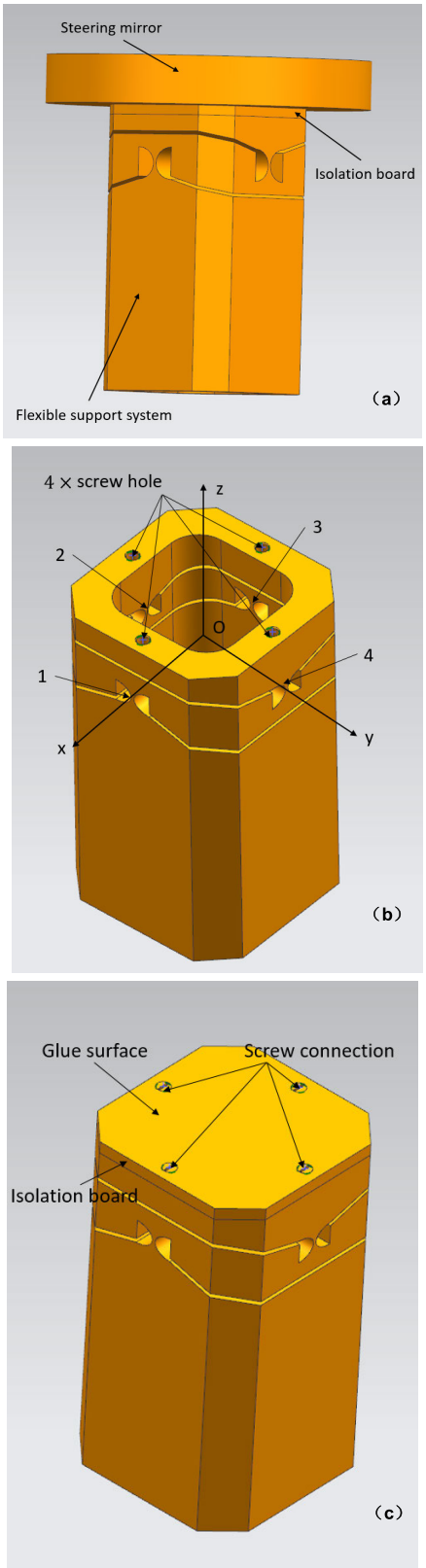

FIGURE 1. (a) The overall structure of the FSM (b) Flexible support system structure (c) Component connection method.

The coordinate system in Figure 2 is O'-x'y'z', which is suitable for single deep cut flexure hinge. In the figure, h is the

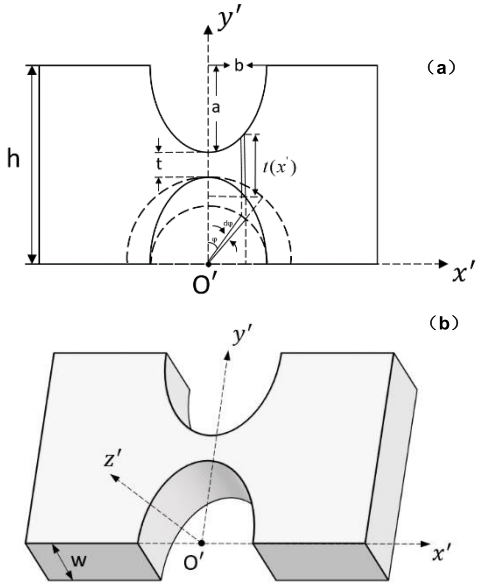

FIGURE 2. (a) Floor plan of deep-cut flexure hinge; (b) Schematic diagram of deep-cut flexure hinge.

height of the flexure hinge, w is the width of the flexure hinge, and t is the minimum cutting thickness of the flexure hinge. The major axis and minor axis of elliptical incision are a and b respectively. We use ANSYS workbench 19.2 to perform modal analysis on the FSM system and the boundary condition is that the bottom of FSM system is fixed. In order to ensure the reliability of the finite element simulation results, we have conducted multiple tests and determined that the mesh size is half of the minimum cutting thickness t. In the following, all our finite element simulation analyses will use this mesh size.

The results of modal analysis of FSM system are shown in Figure 3.

As shown in Fig. 3(a), Fig. 3(b) and Fig. (c), the first three modes of vibration of the FSM system are deflection around the x, y axis and twist around the z axis. As show in Fig. 3(d), when the system deflects around the x-axis, the parallel hinges 1 and 3 bend around radial direction the x' axis, and the parallel hinges 2 and 4 deflect around the radial direction of y', and then they are combined in series to form the deflection of the system around the x-axis. Similarly, when the system deflects around the y-axis, the parallel hinges 2 and 4 bend around the y' axis, the parallel hinges 1 and 3 bend around the radial direction of x', and then the two are combined in series to form the deflection of the system around the y-axis. As show in Fig. 3(e), when the system rotates around the z-axis, the moment is decomposed into four tangential forces distributed on the top of the four parallel hinges. The four tangential forces deflect the four hinges. The parallel deflection of the four hinges is the twist of the system around the z axis.

Therefore, the 2-DOF flexible support system can be simplified to a spring series-parallel model, and the stiffness calculation in the mode shape direction can be performed [18].

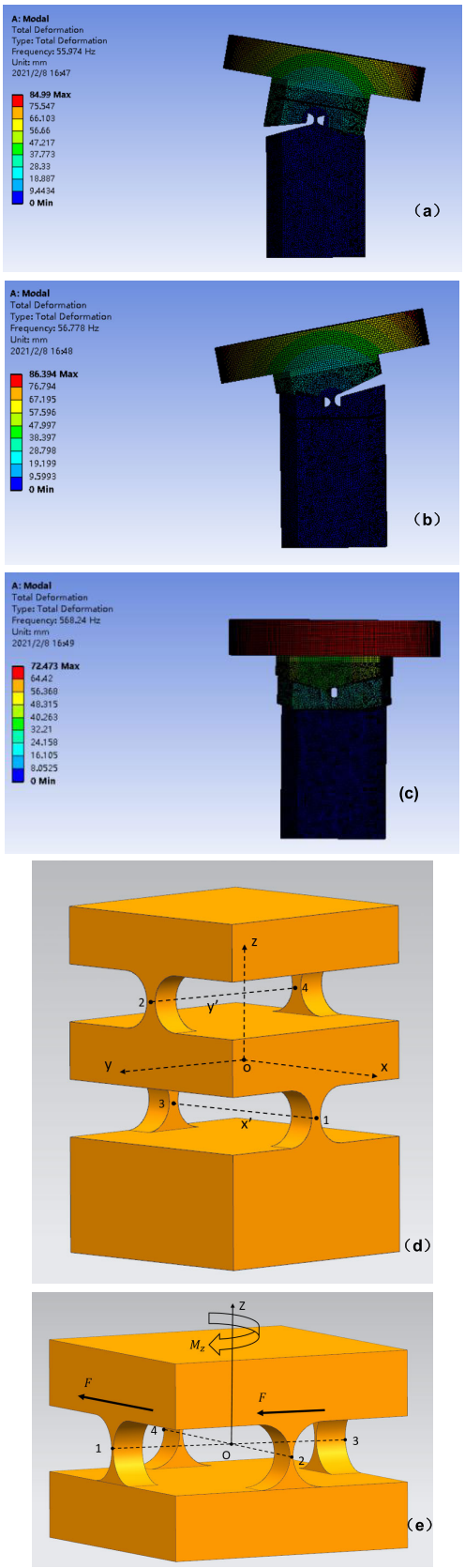

FIGURE 3. (a) First-order vibration mode; (b) Second-order vibration mode; (c) Third-order vibration mode; (d) Simplified schematic diagram of system deflection around x and y axis; (e) Simplified diagram of the system twisting around the z axis.

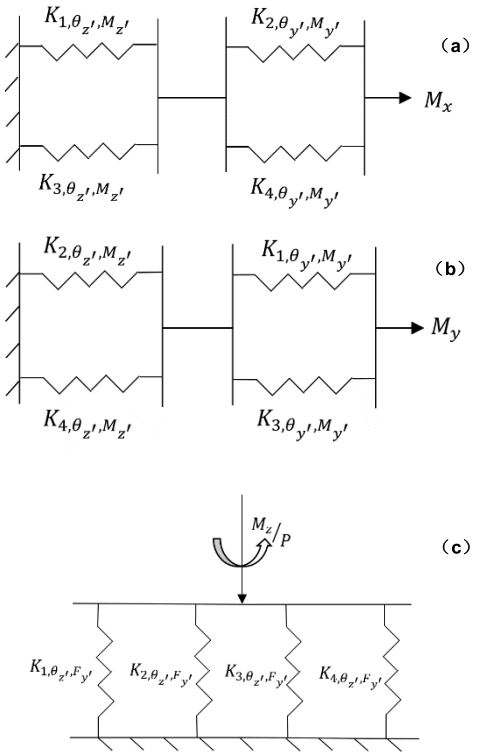

FIGURE 4. (a) Simplified diagram of first-order vibration mode stiffness (b) Simplified diagram of second-order vibration mode stiffness (c) Simplified diagram of third-order vibration mode stiffness.

(1) The first vibration mode: rotating around the x axis

The rotational stiffness around the x-axis is composed of the stiffness of hinges 1, 3 in parallel and the stiffness of hinges 2, 4 in parallel; the two are connected in series [18]. The simplified model is shown in Fig. 4(a). The calculation formula is as follows:

$$\frac{1}{K_x} = \frac{1}{K_{1,\theta_{z'},M_{z'}} + K_{3,\theta_{z'},M_{z'}}} + \frac{1}{K_{2,\theta_{y'},M_{y'}} + K_{4,\theta_{y'},M_{y'}}} \tag{1}$$

The calculation result is:

$$K_x = \frac{(K_{1,\theta_{z'},M_{z'}} + K_{3,\theta_{z'},M_{z'}})(K_{2,\theta_{y'},M_{y'}} + K_{4,\theta_{y'},M_{y'}})}{(K_{1,\theta_{z'},M_{z'}} + K_{3,\theta_{z'},M_{z'}} + K_{2,\theta_{y'},M_{y'}} + K_{4,\theta_{y'},M_{y'}})} \tag{2}$$

(2) The second vibration mode: rotating around the y axis

The rotational stiffness around the y-axis is composed of the stiffness of hinges 2, 4 in parallel and the stiffness of hinges 1, 3 in parallel; the two are connected in series [18]. The simplified model is shown in Fig. 4(b). The calculation formula is as follows:

$$\frac{1}{K_y} = \frac{1}{K_{2,\theta_{z'},M_{z'}} + K_{4,\theta_{z'},M_{z'}}} + \frac{1}{K_{1,\theta_{y'},M_{y'}} + K_{3,\theta_{y'},M_{y'}}} \tag{3}$$

The calculation result is:

$$K_y = \frac{(K_{2,\theta_{z'},M_{z'}} + K_{4,\theta_{z'},M_{z'}})(K_{1,\theta_{y'},M_{y'}} + K_{3,\theta_{y'},M_{y'}})}{(K_{2,\theta_{z'},M_{z'}} + K_{4,\theta_{z'},M_{z'}} + K_{1,\theta_{y'},M_{y'}} + K_{3,\theta_{y'},M_{y'}})} \tag{4}$$

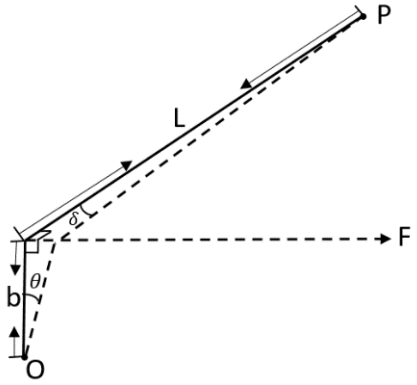

FIGURE 5. Simplified model of third-order vibration mode stiffness.

(3) The Third-Order Mode: Twisting around the z axis

The commonly used formula for calculating the third-order vibration mode of a2-dof fsm system is

$$K_{\theta_z} = 4LK_{\theta_{z'},F_{y'}} \tag{5}$$

When the flexible support system faces the torque M_z around the z-axis, the shear force M_z distributed on the four hinges is $F = M_z/L$, where L is the distance from the deflection center of the flexible hinge to the deflection center of the flexible support system (the system deflection radius). However, it can be inferred from the third-order motion form of the FSM system that K_{θ_z,F_y} can only express the deflection angle of the flexible hinge around the y-axis under tangential force, and it is not on the same plane as the deflection of the FSM system around the z-axis. The simplified model is shown in Fig. 5.

In Fig. 5, point O is the deflection center of the flexible hinge, b is the short semi-axis length of the flexible hinge, L is the length L from the flexible hinge to the rotation center of the support system, P is the rotation center of the support system, and F is the tangential force of the flexible hinge. The K_{θ_z,F_y} in the traditional formula can only represent the deflection angle θ when subjected to tangential force, and the torsion angle generated by the third-order mode of the system is δ. So $4LK_{\theta_z,F_y}$ in the traditional formula cannot represent the torsional stiffness of the system.

According to the geometric relationship in Fig. 5, we can get:

$$b\tan\theta = L\tan\delta \tag{6}$$

Because it is a small deformation, there are:

$$\begin{aligned}\tan\theta &\approx \theta \\ \tan\delta &\approx \delta\end{aligned} \tag{7}$$

Therefore:

$$K_{\theta_{z'},F_{y'}} = \frac{F}{\theta} = \frac{F}{(\frac{L}{b}\cdot\delta)} = \frac{b}{L}\cdot\frac{F}{\delta} = \frac{b}{L}\cdot K_{\delta_z,F_{y'}} \tag{8}$$

Among them, $K_{\delta_z,F_{y'}}$ represents the deflection angle of a single flexible hinge around the deflection center of the support system under the action of a unit tangential force F. Therefore, the torsional stiffness around the z-axis is composed of the stiffness $K_{\delta_z,F_{y'}}$ of the four hinges in parallel. The simplified model is shown in Fig. 3(c), so the calculation formula is:

$$\begin{aligned}\mathrm{K}_{\theta_z} &= \frac{\mathrm{M_z}}{\delta_z} \\ &= \frac{\mathrm{FL}}{\delta_z} \\ &= L(\mathrm{K}_{1,\delta_z,\mathrm{F}_{y'}} + \mathrm{K}_{2,\delta_z}, \mathrm{F}_{y'} + \mathrm{K}_{3,\delta_z,\mathrm{F}_{y'}} + \mathrm{K}_{4,\delta_z,\mathrm{F}_{y'}})\end{aligned} \tag{9}$$

The calculation result is:

$$K_{\theta_z} = 4LK_{\delta_z,F'_y} = 4\frac{L^2}{b}K_{\theta_{z'},F_{y'}} \tag{10}$$

B. DETIVATION OF THE THEORETICAL FORMULA FOR BENDING STIFFNESS OF DEEP-CUT ELLIPTICAL FLEXURE HINGE

We define the force and bending moment on the flexible hinge as$F = [F_{x'}\ F_{y'}F_{z'}M_{x'}M_{y'}\ M_{z'}]^T$, and the corresponding hinge deformation as $D = [\delta_{x'}\delta_{y'}\delta_{z'}\theta_{x'}\theta_{y'}\ \theta_{z'}]^T$. According to the theory of material mechanics, the relationship between them is [18]:

$$D = CF \tag{11}$$

where C is the flexibility matrix of the flexible hinge. And the formula is

$$C = \begin{bmatrix} \frac{\delta_{x'}}{F_{x'}} & 0 & 0 & 0 & 0 & 0 \\ 0 & \frac{\delta_{y'}}{F_{y'}} & 0 & 0 & 0 & \frac{\delta_{y'}}{M_{z'}} \\ 0 & 0 & \frac{\delta_{z'}}{F_{z'}} & 0 & \frac{\delta_{z'}}{M_{y'}} & 0 \\ 0 & 0 & 0 & \frac{\theta_{x'}}{M_{x'}} & 0 & 0 \\ 0 & 0 & \frac{\theta_{y'}}{F_{z'}} & 0 & \frac{\theta_{y'}}{M_{y'}} & 0 \\ 0 & \frac{\theta_{z'}}{F_{y'}} & 0 & 0 & 0 & \frac{\theta_{z'}}{M_{z'}} \end{bmatrix} \tag{12}$$

According to the literature [22], the bending strain energy formula in the working direction of the flexible hinge is:

$$\mathrm{U} = \frac{1}{2}\left(\int_t \frac{F_{x'}^2}{EA(x')}dx' + \int_t \frac{M_{z'1}^2}{EI(x')}dx'\right) \tag{13}$$

With:

$$\begin{cases} M_{z'1} = M_{z'} + F_{y'}x' \\ A(x') = wt(x') \end{cases}$$

where E is the Young modulus of the flexure hinge material, $I(x')$ is the moment of inertia of the flexure hinge section to the central axis, $F_{x'}$ is the tensile force on the free end of the hinge along the x'-axis, and Mz' is the sum of the torque caused by the tangential force along the y'-axis on the free

end of the hinge and the torque around the z-axis. We analyze the torque around the z' axis caused by the rotational moment $M_{z'1}$. According to the Castigliano's second theorem, the calculation formula for the rotation angle of the flexible hinge is [18]:

$$\theta_{z'1} = \frac{\partial U}{\partial M_{z'1}} \tag{14}$$

According to Fig. 5(b)

$$\begin{aligned} I(x') &= \frac{wt(x')^3}{12} \\ t(x') &= 2a + t - \cos\varphi \end{aligned} \tag{15}$$

Substituting (15) into (13), the strain energy of the flexible hinge can be obtained as:

$$U = \frac{6M_{z'}^2}{wE} \int_{-\frac{\pi}{2}}^{\frac{\pi}{2}} \frac{1}{t(x')^3} dx' \tag{16}$$

Substituting (16) into (14), the turning angle can be obtained as:

$$\theta_{z'1} = \frac{\partial U}{\partial M_{z'1}} = \frac{12M_{z'}}{wE} \int_{-\frac{\pi}{2}}^{\frac{\pi}{2}} \frac{1}{t(x')^3} dx' \tag{17}$$

Substituting (17) into (12), the flexibility in the working direction of the flexible hinge can be calculated as:

$$\begin{aligned} C_{\theta_{z'},M_{z'}} &= \frac{\theta_{z'}}{M_{z'}} \\ &= \frac{12b}{wE} \int_{-\frac{\pi}{2}}^{\frac{\pi}{2}} \frac{\cos\varphi}{(2a + t - 2a \cdot \cos\varphi)^3} d\varphi \end{aligned} \tag{18}$$

Suppose $p = \frac{a}{t}$, then:

$$C_{\theta_{z'},M_{z'}} = \frac{12b}{Ewt^3} \int_{-\frac{\pi}{2}}^{\frac{\pi}{2}} \frac{\cos\varphi}{(2p + 1 - 2p \cdot \cos\varphi)^3} d\varphi \tag{19}$$

Let $Y = \int_{-\frac{\pi}{2}}^{\frac{\pi}{2}} \frac{\cos\varphi}{(2p+1-2p\cdot\cos\varphi)^3} d\varphi$, we fund the Y integration result is so complicated, that we can hardly apply it to the optimization design of engineering. So, the method of nonlinear curve fitting is adopted to simplify Y. The goodness of curve fitting is judged by residual sum of squares due to error (SSE), coefficient of determination (R-Square), adjusted coefficient of determination (Adjusted R-Square), root mean square error (RMSE) and residual distribution graphs. The closer the residual sum of squares and the root mean square error are to 0, the closer the determination coefficient and the adjusted determination coefficient are to 1, the better the curve fit [18].

A power function fitting is used for the Y function. As shown in the figure, from the residual distribution diagram and various determination coefficients, it can be seen that the power function fitting results are better and meet the error requirements.

The fitting result is:

$$Y = 1.079p^{-0.4753} \tag{20}$$

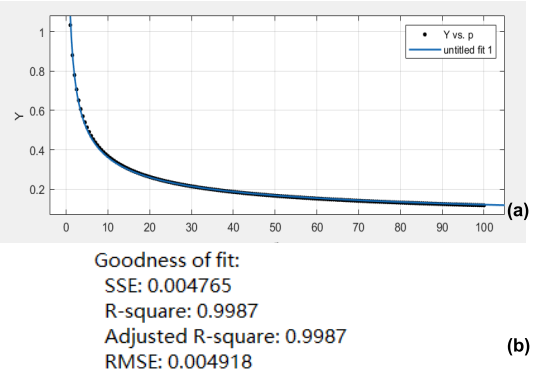

FIGURE 6. (a) Non-linear fitting curve diagram; (b) Non-linear fitting determination coefficient.

Then the flexibility in the working direction of the deep-cut flexible hinge is:

$$C_{\theta_{z'},M_{z'}} = \frac{12b \times 1.079p^{-0.4753}}{Ewt^3} \tag{21}$$

Combining the calculation of the flexibility matrix of the elliptical arc flexure hinge in the literature [18], and using the elastic deformation theory and nonlinear fitting simplification, the flexibility calculation formulas in other secondary directions can be calculated, and the results are as follows:

$$C_{\theta_{y'},M_{y'}} = \frac{12b}{Ew^3t}[2.268(\frac{a}{t})^{-0.1878} - 0.6993] \tag{22}$$

$$C_{\theta_{z'},F_{y'}} = \frac{12b^2}{Ewt^3}[1.079(\frac{a}{t})^{-0.4753}] \tag{23}$$

C. DERIVATION OF THE THEORETICAL CALCULATION FORMULA FOR THE MOMENT OF INERTIA OF THE FSM SYSTEM

The moment of inertia of the FSM system about its deflection axis discussed in this paper is mainly composed of two parts, including an irregular support structure part and a regular mirror structure part. Moreover, the moment of inertia of the three vibration mode is quite different. So, it is necessary to discuss them separately.

(1) Calculation of the moment of inertia of the FSM system twisted around the x and y axes

Torsion around the x-axis is the first-order vibration mode direction of the system, and torsion around the y-axis is the second-order vibration mode direction of the system. The rotation centers of the four flexure hinges are in the same plane, so the distances from the x and y axes to the bottom of the reflector are equal. The schematic diagram is shown in Figure 7, where h is the thickness of the mirror, and z is the distance from the bottom of the mirror to the x-axis and y-axis.

Because the mirror part and the supporting structure part are twisted around the same axis, the moment of inertia J_x and J_y of the system around the x and y axes are:

$$\begin{cases} J_x = J_{xd} + J_h \\ J_y = J_{yd} + J_h \end{cases} \tag{24}$$

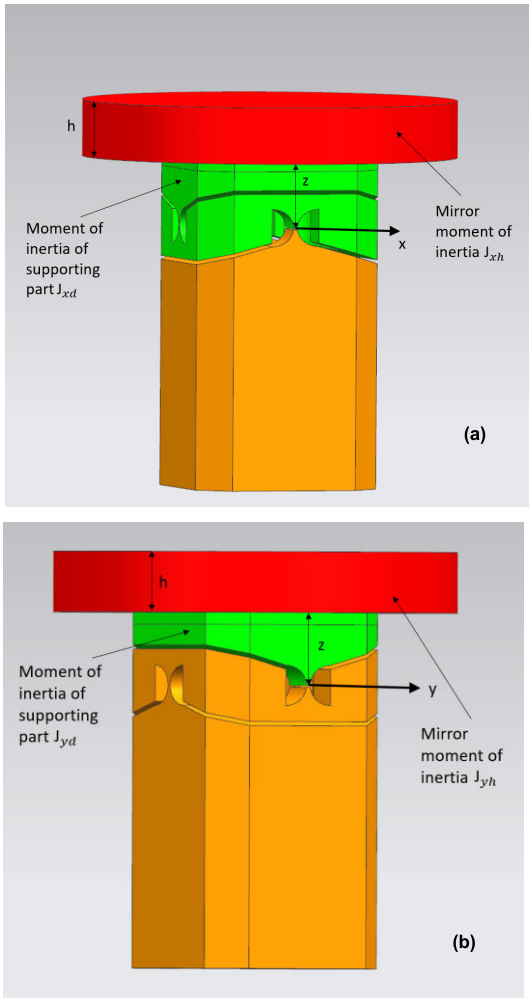

FIGURE 7. (a) Moment of inertia about the x axis (b) Moment of inertia about the y axis.

where J_{xd} is the moment of inertia of the flexible supporting part, and J_{xh} is the moment of inertia of a regular cylinder around a fixed axis. Based on this, the numerical relationship between J_{xh} and the mirror thickness h can be obtained. According to the formula of the moment of inertia of the cylinder and the parallel axis theorem, J_{xh} is:

Among them, J_{xd} and J_{yd} are the moments of inertia of the flexible supporting part, which are obtained by measurement. J_h is the moment of inertia of a regular cylinder around a fixed axis, so the numerical relationship between J_h and the mirror thickness h can be obtained. According to the formula of the moment of inertia of the cylinder and the parallel axis theorem, J_h can be obtained as:

$$J_h = \frac{1}{12}m(3r^2 + h^2) + m \cdot (\frac{h}{2} + z)^2 = \pi r^2 h\rho(\frac{r^2}{4} + \frac{h^2}{3} + z^2 + z \cdot h) \quad (25)$$

where r is the radius of the reflector and ρ is the density of the reflector.

(2) Calculation of the moment of inertia of the FSM system twisted around the z axis

Around the z axis is the third-order vibration mode direction of the system, as shown in Fig. 8:

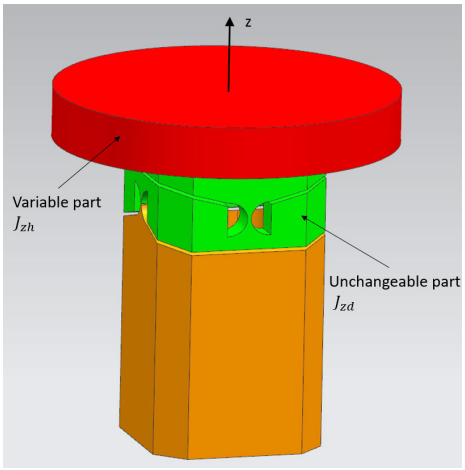

FIGURE 8. Moment of inertia about the z axis.

In the same way, the moment of inertia around the z-axis is composed of two parts: the moment of inertia of the irregular support part and the moment of inertia of the cylindrical mirror around the fixed axis, so:

$$J_z = J_{zd} + J_{zh} \quad (26)$$

Among them, the calculation formula of J_{zh} is

$$J_{zh} = \frac{1}{2}mr^2 = \frac{1}{2}\pi r^4 h\rho \quad (27)$$

D. DERIVATION OF THEORETICAL CALCULATION FORMULA FOR NATURAL FREQUENCY OF FLEXIBLE SUPPORT SYSTEM

According to the results of the modal analysis, the first two natural frequency modes of the FSM system are the torsional vibration motions around the x and y axes. It can be simplified to a single degree of freedom torsional vibration model. According to the literature [18], [20] the relationship between the stiffness of the model in the torsional vibration direction and the natural frequency in this direction can be expressed as:

$$f_{n1,2} = \frac{1}{2\pi}\sqrt{\frac{K_{\theta n}}{J_n}} \quad (28)$$

where $K_{\theta n}$ is the torsional stiffness in the direction of motion, and J_n is the moment of inertia in the direction of motion.

The third-order vibration mode of the FSM system is torsion around the z-axis. Because it is a small deformation motion, it can be simplified to a single degree of freedom torsional vibration. The newly derived third-order vibration mode of stiffness calculation formula in the direction into

TABLE 1. Comparison of theoretical calculation and finite element simulation of working stiffness of deep-cut flexure hinge.

a(mm)	b(mm)	t(mm)	w(mm)	Theoretical calculation results（N*m/rad）	Finite element simulation results（N*m/rad）	Error percentage （%）
8	6	1	8	30.4346	30.3674	0.22
8	4	1	8	45.6519	42.3012	7.9
5	4	1	8	36.5124	35.5577	2.7
5	4	0.5	8	6.3450	6.5876	-3.7
5	4	0.5	5	3.9656	4.0606	-2.4
5	2	0.5	5	7.9312	7.2922	8.8

the calculation, the third-order natural frequency calculation formula is:

$$f_{n3} = \frac{1}{2\pi}\sqrt{\frac{K_{\theta_z}}{J_z}} \tag{29}$$

where K_{θ_z} is the torsional stiffness of the system around the z-axis, and J_z is the torsional stiffness of the moving part around the z-axis.

III. THE FINITE ELEMENT VERIFICATION OF THE THEORETICAL CALCULATION FORMULA FOR THE WORKING STIFFNESS OF THE FLEXIBLE HINGE AND THE THIRD-ORDER NATURAL FREQUENCY THEORETICAL CALCULATION FORMULA

A. THE FINITE ELEMENT SIMULATION VERIFICATION OF THE THEORETICAL CALCULATION FORMULA OF THE WORKING STIFFNESS OF THE DEEP-CUT FLEXURE HINGE

The deep cut flexure hinge is modeled in Unigraphics NX and imported into Ansys for finite element simulation verification, as shown in Fig. 9

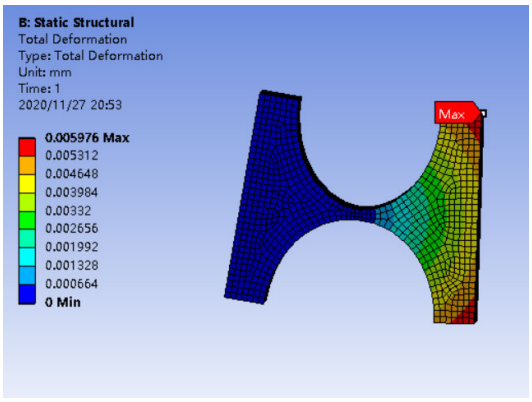

FIGURE 9. Finite element simulation of deep-cut flexure hinge.

The results show that the error between the theoretical formula calculation result and the finite element simulation result does not exceed 9%, which proves the accuracy of the theoretical deduction result. The results are shown in Tab. 1

B. FINITE ELEMENT VERIFICATION OF THE THIRD-ORDER NATURAL FREQUENCY CALCULATION FORMULA OF THE FSM SYSTEM

The FSM system is modeled in Unigraphics NX and imported into Ansys for finite element simulation verification, as shown in Fig. 10.

The finite element simulation results are shown in Tab. 2. According to the finite element simulation results, the error between the theoretical formula and the finite element simulation results is not more than 9%, which proves the derived stiffness calculation formula, the mirror moment of inertia calculation formula and the first to third order natural frequency calculation formula are accurate.

C. SENSITIVITY ANALYSIS OF STRUCTURAL PARAMETERS OF THE FSM

The parameter sensitivity analysis of optimization problems is to clarify the relationship between the design variables and the objective function.It is of great significance for the determination of the initial variables and the improvement of the optimization effect. In this paper, the Sobol algorithm is used to analyze the sensitivity of the four structural parameters a, b, t, and h of the FSM system to the first three-order natural frequencies.

Sobol is a global sensitivity analysis method based on variance. It quantitatively evaluates the influence of each input parameter and the interaction between parameters on the output variable by decomposing the variance of the output variable. In this study, Sobol's global SA was performed using the Matlab R2019 (The Math Works Inc.: Natick, MA, USA). Within the given parameter variation range, the influence degree of each structural parameter on the 1st $\sim$ 3rd order natural frequency is analyzed.

If $y = f(X_1, X_2, \cdots, X_m)$ represents the model structure, $X_1, X_2, \cdots, X_m$ represent the model parameters, and

TABLE 2. Comparison of theoretical calculation and finite element simulation of first to third-order natural frequency of FSM system.

a(mm)	b(mm)	w(mm)	t(mm)	Mirror thickness:h(mm)	First-order natural frequency error （%）	Second-order natural frequency error （%）	Third-order natural frequency error （%）
4	3.5	5	0.8	23	0.1	8.97	0.61
4.6	3	8	1	19	-0.63	1.05	3.69
6	5	8	1	15	-6	-5.8	1.68

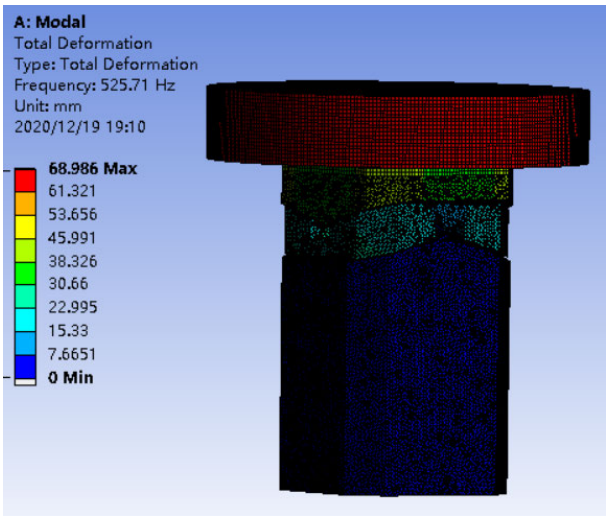

FIGURE 10. vibration mode simulation diagram.

m represents the number of model parameters, the variance decomposition formula can be expressed as:

$$V(y) = \sum_{i=1}^{m} V_i + \sum_{i<j<m}^{m} V_{ij} + \sum_{i<j<k<m}^{m} V_{ijk} \cdots + V_{1,2,\cdots,m} \tag{30}$$

where: $V(y)$ is the total variance of the model output y; V_i is the variance produced by the parameter X_i; V_{ij} is the variance produced by the interaction of parameters X_i and X_j; V_{ijk} is the variance produced by the interaction of parameters X_i, X_j and X_k; $V_{1,}2,_{\ldots,}m$ is the variance produced by the combined action of m parameters [23].

For parameter X_i, the first-order sensitivity index S_i can be used to express the direct contribution rate of parameter X_i to the total variance of the model simulation results [23]. The specific formulas can be expressed as:

$$S_i = \frac{V_i}{V(y)} \tag{31}$$

Based on the Latin hypercube sampling method, 10,000 points are selected in the design variable area.And the first-order sensitivity of the 1st to 3rd order natural frequencies of the system are analyzed respectively. The results are shown in Fig. 11.

For the first and second natural frequencies of the FSM system, the sensitivity index of the long and short semi-axes a and b of the flexure hinge, the thickness of the mirror h, and the minimum cutting thickness t of the flexure hinge are arranged in increasing order. It means that the influence of the reflector thickness on the natural frequency is greater than the long and short semi-axes a and b of the flexible hinge.

From the above analysis results, it can be seen that for the first and second natural frequencies of the FSM system, the first-order sensitivity index of the minimum cutting thickness t of the flexure hinge is the largest, followed by the mirror thickness h, and the long and short semi-axes a, b The impact is relatively small. For the third-order natural frequency, the first-order sensitivity index of the minimum cutting thickness t and the short semi-axis length b is larger. The sensitivity index of the mirror thickness h is smaller than the former two, but much larger than the semi-major axis a. From the above analysis, it can be seen that compared with the design variables a, b, and t that are often used in the optimization design of traditional flexure hinges, the thickness h of the mirror that is rarely considered has a greater impact on the natural frequency of the system. Therefore, when we optimize the design of the natural frequency of the system, the reflector thickness h is introduced into the optimization function for analysis

IV. MULTI-OBJECTIVE OPTIMIZATION DESIGN EXAMPLE OF FSM

The diameter of the FSM is 100 mm and the thickness of the isolation plate is 3 mm. The deflection range of the FSM system is ±3mrad, and the repeated positioning accuracy is $\delta_p \leq 8urad$. The material of flexible support system is TC4, the material of isolation plate is indium steel, and the material of reflector is glass-ceramic. The modal analysis of the initial structure was carried out. The first to third natural frequencies and initial structural parameters are shown in Tab. 3. The parameters a, b, t, h are independent variables, which are used to optimize the objective function.

A. OBJECTIVE FUNCTION

In order to improve the control bandwidth of the system, the natural frequency of the system structure is required to be 2 ∼ 4 times higher than the control bandwidth of the

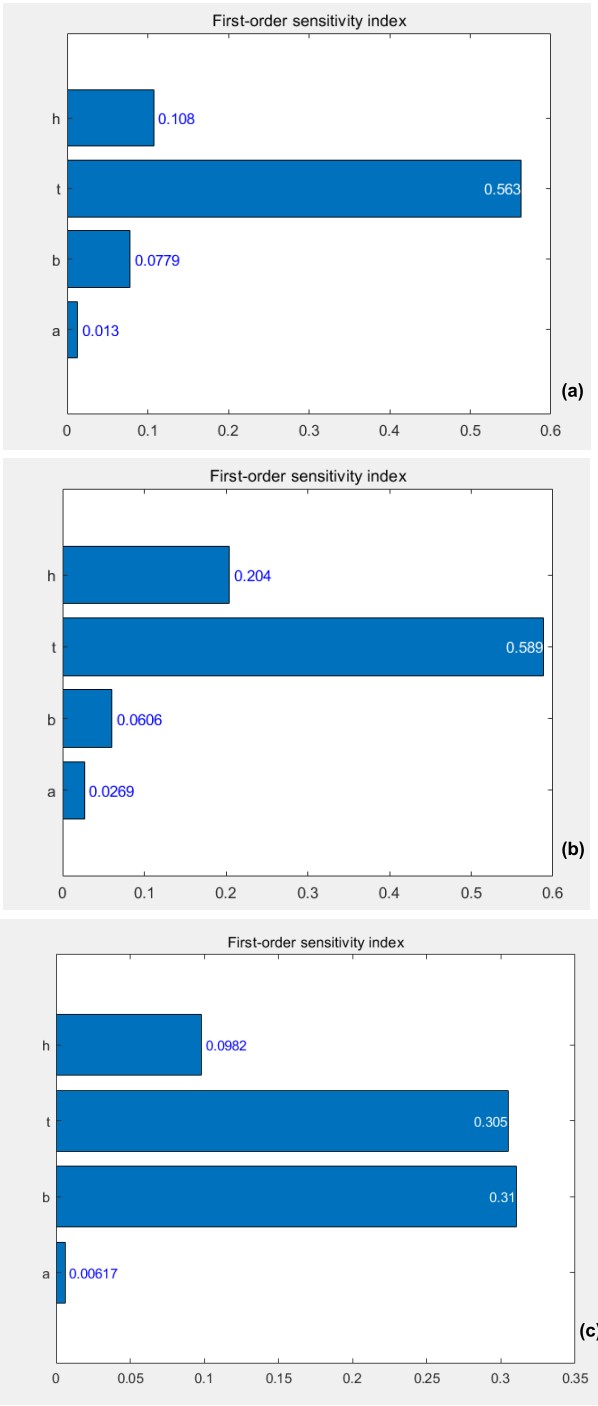

FIGURE 11. (a) First-order natural frequency sensitivity analysis (b) Second-order natural frequency sensitivity analysis (c) Sensitivity analysis of third-order natural frequency.

system. However, such a design will lead to excessive low-order natural frequency of the system, and the stiffness in the working direction of the system will be too large, which will greatly increase the burden of the system driver [18]. Therefore, the following design methods are adopted: on the one hand, the low-order natural frequency in the working direction of the system should be reduced as much as possible, and it can be suppressed by the control system. On the other hand, the higher-order natural frequency in the non-working direction of the system is increased as much as possible to improve the control bandwidth of the system [19].

According to (28) and (29), the specific numerical relationship between the third-order natural frequency $f_{n_{1\sim3}}$, the three-axis rotational stiffness $K_{\theta n}$ and the three-axis rotational inertia J_n of the flexible support system can be obtained. Because the size change of flexure hinge has little influence on the inertia of flexible support structure, the inertia of system support structure is set as a fixed value to facilitate the optimization calculation. Therefore, the following multi-objective optimization function is constructed:

$$Object = \begin{cases} \min f_{n1}(x) \\ \min f_{n2}(x) \\ \max f_{n3}(x) \end{cases} \tag{32}$$

In multi-objective optimization, the result obtained by the multi-objective optimization algorithm is generally an optimal solution set, that is, Pareto solution set. Therefore, it is necessary to confirm the weighted value according to the importance of each sub objective and multiple parameter adjustments, so as to finally calculate a group of optimal solutions [24]. In the optimization calculation of natural frequency, the upper limit of natural frequency in low order working direction is determined by the second-order natural frequency, and the lower limit of natural frequency of higher-order non-working direction is determined by the third-order natural frequency. According to the design idea of FSM system to increase the natural frequency in the non-working direction and reduce the natural frequency in the working direction, it is important to increase the third-order natural frequency while reducing the second-order natural frequency. Therefore, the two sub objectives occupy a more important position in the optimization function, and a larger weight value should be given when the weight is allocated. Let the weighting coefficients of natural frequencies of order 1-3 are respectively. According to the above requirements, the parameters are adjusted, and the weighted coefficients of natural frequencies of order 1-3 are obtained as follows:$\beta_1 = 0.2$, $\beta_2 = 0.3$, $\beta_3 = 0.5$.

After determining the weighted coefficient, the relative sorting method is used to find the optimal solution in the Pareto solution set. Assuming that the order of the natural frequencies represented by each solution x_n in the Pareto solution set is $\mathrm{R}_1(x_n)$, $\mathrm{R}_2(x_n)$, $\mathrm{R}_3(x_n)$, then the relative order $\mathrm{R}(x_n)$ of the x_n in the Pareto solution set is $\mathrm{R}(x_n) = \beta_1\mathrm{R}_1(x_n) + \beta_2\mathrm{R}_2(x_n) - \beta_3\mathrm{R}_3(x_n)$. The optimal solution in the Pareto solution set is the one with the smallest $\mathrm{R}(x_n)$ [24].

B. CONSTRAINED CONDITION

When the flexure hinge is bent, the maximum stress of the hinge appears at the minimum cutting thickness t of the hinge, which has the effect of stress concentration. Therefore, according to the pure bending theory in material mechanics,

TABLE 3. The first to third natural frequencies and initial structural parameters.

a(mm)	b(mm)	t(mm)	w(mm)	L(mm)	D(mm)	h(mm)	f_1 (Hz)	f_2 (Hz)	f_3 (Hz)
10	8	1	8	25	100	15	60.715	60.814	236.93

the maximum stress of flexure hinge is:

$$\sigma_{\max} = K_t \frac{6M_{\max}}{t^2 w} \tag{33}$$

where K_t is the factor of stress concentration [25] and M_{max} is the external torque applied to the hinge at the maximum deflection angle. The calculation formula is as follows:

$$\begin{cases} K_t = (1 + \dfrac{at}{2b^2})^{\frac{9}{20}} \\ M_{\max} = \dfrac{Ewt^3 \cdot 10^{-3}}{4.316bp^{-0.4753}} \end{cases} \tag{34}$$

Substituting (35) into (34), we can get the following results:

$$\sigma_{\max} = (1 + \frac{at}{2b^2})^{\frac{9}{20}} \times \frac{6Et \cdot 10^{-3}}{4.316b(\frac{a}{t})^{-0.4753}} \tag{35}$$

The yield strength of TC4 is 4.3×10^8 Pa and the safety factor is 2.745. Yield strength and safety factor are substituted into (36):

$$c_1(x) = (1 + \frac{at}{2b^2})^{\frac{9}{20}} \times \frac{6Et \cdot 10^{-3}}{4.316b(\frac{a}{t})^{-0.4753}} - \frac{4.3 \times 10^2}{2.745} \leq 0 \tag{36}$$

(2) Inequality constraints on kinematic accuracy of flexure hinges

In the analysis of the kinematic accuracy of flexure hinge, the displacement of the geometric center of the flexure hinge, that is, the displacement of the deflection center of the flexure hinge, is generally taken as the quantitative index to measure the kinematic accuracy of the flexure hinge [25]. According to the formula of material mechanics, the displacement of the center point can be obtained as follows:

$$yc = \iint \frac{M(x')}{EI(x')} dx' dx' \tag{37}$$

With

$$\begin{cases} I(x') = \dfrac{\mathrm{wt}^3(\mathrm{x}')}{12} \\ M(x') = M \end{cases}$$

Equation (38) is transformed into polar coordinate form:

$$\begin{aligned} &\frac{12\mathrm{Mb}}{\mathrm{Ew}} \int\int \frac{\cos\varphi}{(2\mathrm{a} + \mathrm{t} - 2\mathrm{a}\cos\varphi)^3} \mathrm{d}\varphi \mathrm{b}\cos\varphi \mathrm{d}\varphi \\ &= \frac{12Mb}{Ewt^3} \int_{-\frac{\pi}{2}}^{0} \int_{-\frac{\pi}{2}}^{\varphi} \frac{\cos\beta}{(2p + 1 - 2p\cos\beta)^3} d\beta b\cos\varphi d\varphi \\ &= \frac{6Mb^2}{Ewt^3} \cdot \frac{1}{1 + 2p} \end{aligned} \tag{38}$$

Substituting the repeated positioning accuracy A of the flexure hinge into (38), the constraint expression of the motion accuracy of the flexure hinge can be obtained as:

$$c_2(x) = \frac{6 \times 10^{-3} b}{4.316 \cdot (1 + \frac{2a}{t}) \cdot (\frac{a}{t})^{-0.4753}} - 8 \times 10^{-3} \leq 0 \tag{39}$$

C. OPTIMIZATION CALCULATION

(1) Optimization model

The optimization model is as follows:

$$\begin{aligned} f_{obj} &= \begin{cases} \min \beta_1 f_{n1}(x) \\ \min \beta_2 f_{n2}(x) \\ \max \beta_3 f_{n3}(x) \end{cases} \\ &\text{suppose:x1=a,x2=b,x3=t,} \\ &\qquad \text{x4=h x=(x1,x2,x3,x4)}^T \\ s.t. &\begin{cases} c(x) \leq 0 \\ A \cdot x \leq b \\ lb < x < ub \end{cases} \end{aligned} \tag{40}$$

The long axis a, the minor axis b and the minimum cutting thickness t of the flexure hinge are taken as variables. At the same time, according to the geometric constraints, the linear inequality constraint matrix A is obtained as follows: [0 −1 5 0; −1 0 5 0; 10 −5 0 0; −1 1.2 0 0; 1 −2 0 0], b = [0; 0; 0; 0]. According to the design principle of the mirror, the radius-thickness ratio of the cylindrical mirror should not be less than 10:1, but it should not be too high, otherwise the system load will be too large. The diameter of the mirror studied in this paper is 100 mm. According to the above design philosophy, the thickness of the mirror varies from 13 mm to 23 mm. Therefore, according to the machining accuracy of flexure hinge and the range of mirror thickness, we can get the boundary constraint lb = [0,0,0.8,13], ub = [10; 10; 2; 23]. The nonlinear inequality constraints are strength inequality constraint c_1 and motion accuracy inequality constraint c_2.

(2) Genetic algorithm and its evaluation method

NSGA-II is an improved optimization algorithm based on genetic algorithm proposed by Kalyanmoy Deb in 2002. The main difference between NSGA-II algorithm and common genetic algorithm is that it adopts non dominated stratification and congestion comparison method. Non dominated stratification is to stratify the whole population by comparing the dominance relationships among individuals (If individual Y_i is better than individual Y_j in all optimization objectives, it is called Y_i dominating Y_j). After each iteration, individuals are called in order of dominance layer from high to low

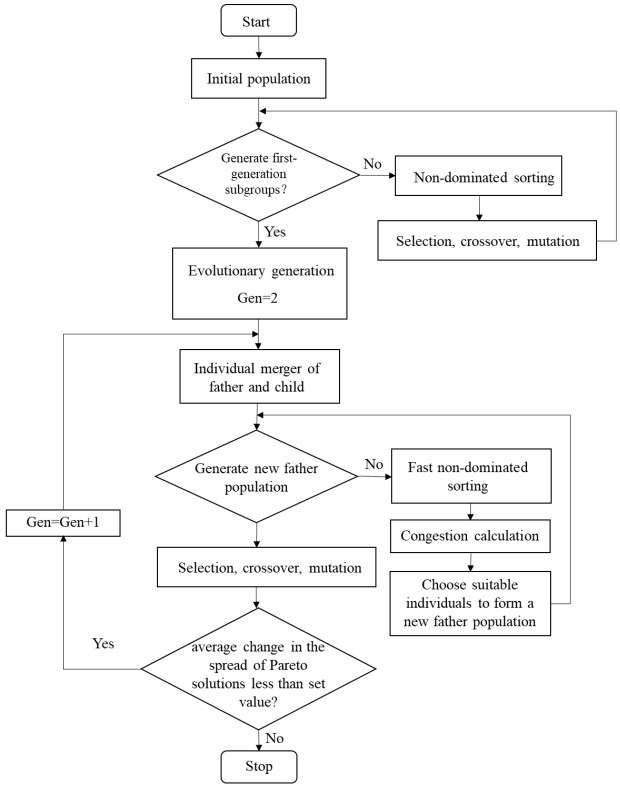

FIGURE 12. NSGA-II optimization flow chart.

in order to generate new species group. If the difference between the number of individuals in the new species group and the number of individuals N is less than the number of individuals in the current dominant layer, the crowding comparison method is used to select better individuals from the current individual layer for filling. Before the start of each iteration, the parent population is combined with the current population to form a new species group with the size of 2N. It is instrumental in ensuring that some excellent individuals will not be discarded during the evolution process [24]. The NSGA-II algorithm optimization process is shown in Fig. 12

(3) Optimization results and analysis verification

In this paper, Matlab is used for optimization calculation, and the optimized initial values are a = 10, b = 8, and t = 1. If the weighted average relative change in the spread of the Pareto solutions over Stall generations is less than $1*10^{-4}$, and the spread is smaller than the average spread over the last Stall generations, then the algorithm stops [24]. The final optimization calculation iterations 106 times, the optimization result are a = 3.9885, b = 3.0145, t = 0.9107, h = 17.3430. In order to facilitate processing, the above optimization results are approximated, and the final optimization result parameters obtained are a = 4, b = 3, t = 0.9, h = 17.

Based on the above optimized structural parameters and the parameters of other key components of the system structure shown before, the UG modeling of the structure was carried out. The three views of the optimized structure are shown in Fig. 13

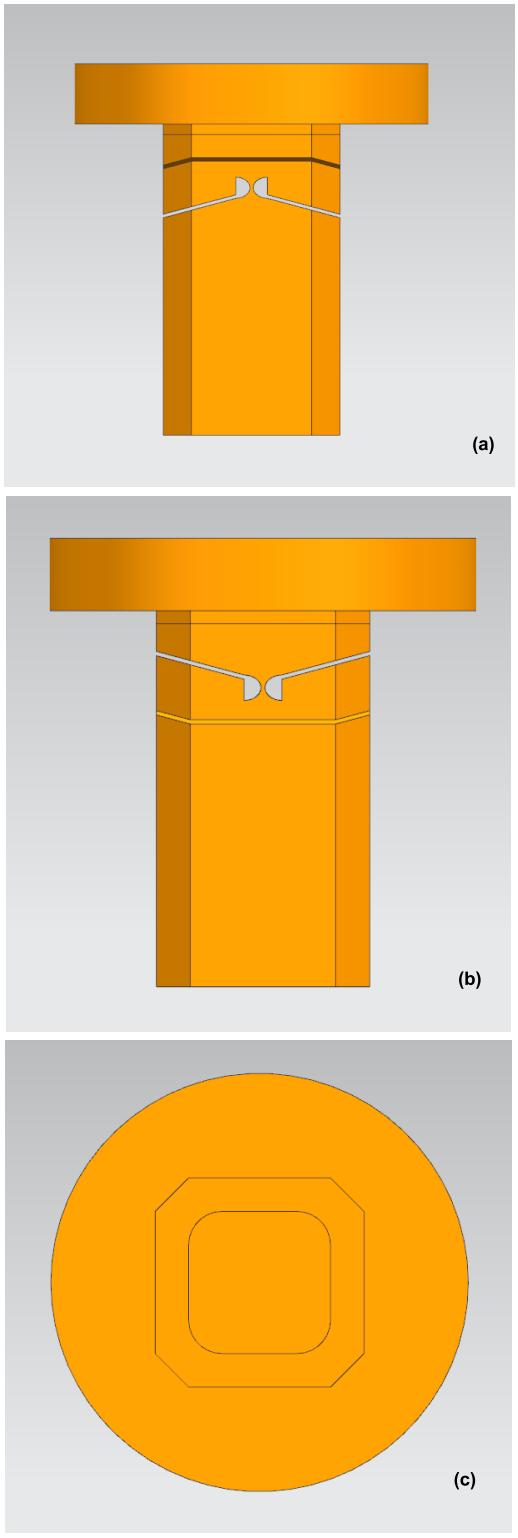

FIGURE 13. (a) Front view; (b) Right view; (c) Bottom view.

The third-order natural frequency of the optimized structure was calculated by using the natural frequency calculation formula derived before, and it was compared with the third-order natural frequency of the initial

TABLE 4. Comparison of system stiffness between multi-objective optimized structure and initial structure.

	a (mm)	b (mm)	t (mm)	h (mm)	f_1 (Hz)	f_2 (Hz)	f_3 (Hz)
Initial value	10	8	1	15	60.715	60.814	236.93
Optimized value	4	3	0.9	17	56.7	57.8	549
Optimization rate					-6.61%	-4.96%	131.71%

structure to preliminarily analyze the effect of optimization calculation. The comparison results are shown in Tab. 4

The above preliminary calculation results show that the first and second order natural frequencies of the optimized structure are reduced by 6.61% and 4.96% respectively, and the third-order natural frequencies are increased by 131.71%. The low-order natural frequency in the working direction is reduced, and the higher-order natural frequency in the non-working direction is further increased, which proves that the optimized structure meets the design requirements initially.

In order to further analyze the natural frequency of the optimized structure and get more intuitive results, the optimized structure is simulated by ANSYS mode, and the results are shown in Fig. 14. The comparison between the simulation results of natural frequency and the theoretical calculation value is shown in Tab. 5. From the analysis results, it can be seen that the error between the theoretical calculation results and the finite element simulation results of the third-order natural frequency is less than 3.4%, which proves the accuracy of the previous theoretical derivation formula again. The comparison between the modal simulation results of the new structure and the initial structure is shown in Tab. 6. Compared with the original structure, the first and second order natural frequencies of the FSM are reduced by 7.8% and 7.11% respectively, which are 55.974hz and 56.778hz respectively. The third order natural frequency is increased by 139.8% and to 568.24hz compared with the original structure. It can be seen that the optimized calculation can achieve the design purpose and meet the design requirements of the FSM system. The third natural frequency, which determines the control bandwidth of the system, has been greatly optimized, which proves the effectiveness of the weighting coefficient. The optimization calculation effectively reduces the low-order natural frequency of the structure in the working direction, and lays a good foundation for adding the control system in the next step, so that the low-order natural frequency of the system can be effectively suppressed. At the same time, the optimal calculation effectively improves the third-order natural frequency of the structure in the non- working direction, so that the system control bandwidth can be significantly increased. It is expected that the control bandwidth of the

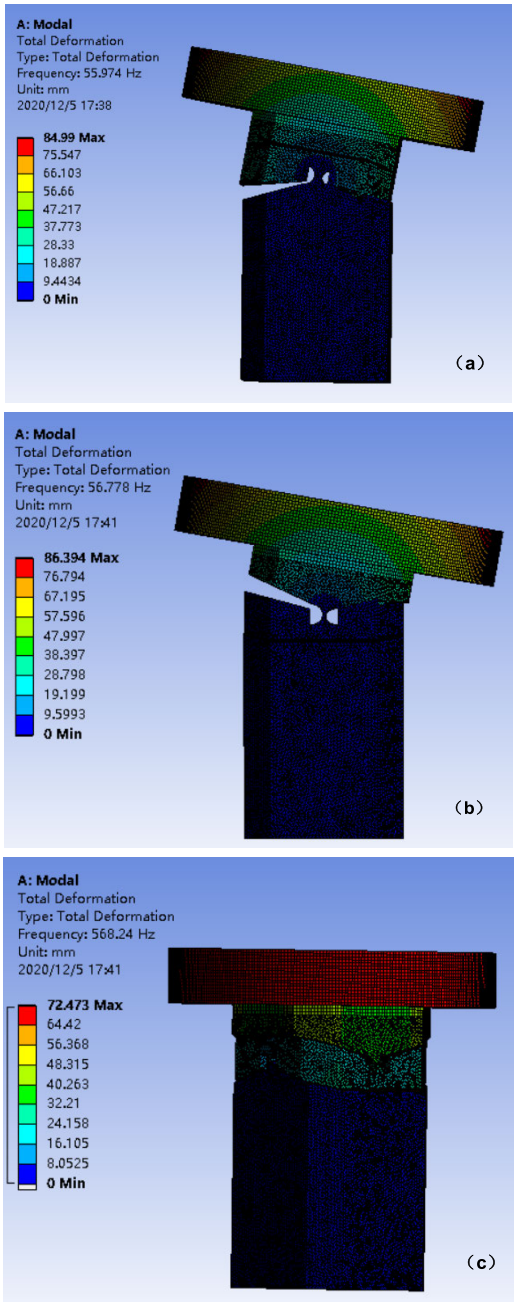

FIGURE 14. (a) First-order mode (b) Second-order mode (c) Third-order mode.

TABLE 5. Comparison of theoretical calculation value and finite element simulation value of structure third-order natural frequency.

	First-order mode (Hz)	Second-order mode (Hz)	Third-order mode (Hz)
Theoretical calculation value	56.7	57.8	549
Finiteelement simulation value	55.974	56.778	568.24
Error percentage	1.3%	1.8%	-3.4%

TABLE 6. Comparison of the fourth-order natural frequency between the optimized structure and the initial structure.

	First-order mode (Hz)	Second-order mode (Hz)	Third-order mode (Hz)
Initial structure	60.715	60.814	236.93
Optimized structure	55.974	56.778	568.24
Optimization rate	-7.8%	-7.11%	139.8%

system can reach more than 300Hz after adding the control system to suppress the low-order frequency.

V. CONCLUSION

In order to optimize the control bandwidth of the deep-cut flexure hinge FSM system based on the 2-DOF, the first to third-order natural frequency of the FSM system was simulated and analyzed by finite element method, and the working stiffness in three vibration mode directions was deduced and analyzed theoretically, which solves the problem that the traditional calculation formula is not suitable for the third mode vibration direction. Next, using the energy method and the Castigliano's second theorem, the calculation formula of the working stiffness for the deep-notch flexure hinge was derived, and it was simplified by using the nonlinear fitting method. The error between the simplified formula and the finite element simulation result is less than 9%, which solves the problem that the traditional formula is too complex. Then, the formula for calculating the relationship between the thickness of the mirror and the moment of inertia in the direction of the vibration mode was derived. The first to third-order natural frequency of the FSM system was calculated by using the above derived working stiffness formula and the moment of inertia in the direction of the vibration mode. It was verified by the finite element simulation. The error between the calculation results and the simulation results is less than 9%, which proves the reliability of the formulas for calculating the working stiffness in first to third-order vibration mode directions, mirror moment of inertia and the first to third-order natural frequency of the system. Finally, the multi-objective optimization design, which is with hinge structure parameters and reflector thickness as independent variables, was carried out with the minimum of the first and second-order natural frequencies and the maximum of the third-order natural frequencies. The obtained optimal structure effectively reduces the first and second-order natural frequencies, and improves the third-order natural frequencies. The finite element verification proves the reliability and effectiveness of the optimization results. The formula and the optimization method presented in this paper are of engineering significance for the improvement of control bandwidth and the theoretical analysis of natural frequency for 2-DOF flexure hinge FSM..

REFERENCES

[1] E. Csencsics and G. Schitter, "System design and control of a resonant fast steering mirror for lissajous-based scanning," *IEEE/ASME Trans. Mechatronics*, vol. 22, no. 5, pp. 1963–1972, Oct. 2017.
[2] C. Tianqing, W. Quandong, Z. Lei, H. Na, and D. Wenjun, "Battlefield dynamic scanning and staring imaging system based on fast steering mirror," *J. Syst. Eng. Electron.*, vol. 30, no. 1, pp. 37–56, Feb. 2019.
[3] Q. Dong, Y. Liu, Y. Zhang, S. Gao, and T. Chen, "Improved ADRC with ILC control of a CCD-based tracking loop for fast steering mirror system," *IEEE Photon. J.*, vol. 10, no. 4, Aug. 2018, Art. no. 6601314.
[4] E. Csencsics, B. Sitz, and G. Schitter, "Integration of control design and system operation of a high performance piezo-actuated fast steering mirror," *IEEE/ASME Trans. Mechatronics*, vol. 25, no. 1, pp. 239–247, Feb. 2020.
[5] E. Csencsics, J. Schlarp, and G. Schitter, "High-performance hybrid-reluctance-force-based tip/tilt system: Design, control, and evaluation," *IEEE/ASME Trans. Mechatronics*, vol. 23, no. 5, pp. 2494–2502, Oct. 2018.
[6] Q. Li, L. Liu, X. Ma, S.-L. Chen, H. Yun, and S. Tang, "Development of multitarget acquisition, pointing, and tracking system for airborne laser communication," *IEEE Trans. Ind. Informat.*, vol. 15, no. 3, pp. 1720–1729, Mar. 2019.
[7] Y. Fan, Y. He, and U.-X. Tan, "Real-time compensation system via gyroscope and fast steering mirror for wide-bandwidth multiple-frequency vehicle disturbance," *IEEE/ASME Trans. Mechatronics*, vol. 25, no. 2, pp. 650–660, Apr. 2020.
[8] C. Deng, T. Tang, Y. Mao, and G. Ren, "Enhanced disturbance observer based on acceleration measurement for fast steering mirror systems," *IEEE Photon. J.*, vol. 9, no. 3, Jun. 2017, Art. no. 6802211.
[9] N. O. Perez-Arancibia, J. S. Gibson, and T.-C. Tsao, "Frequency-weighted minimum-variance adaptive control of laser beam jitter," *IEEE/ASME Trans. Mechatronics*, vol. 14, no. 3, pp. 337–348, Jun. 2009.
[10] J. Tani, S. Mishra, and J. T. Wen, "Identification of fast-rate systems using slow-rate image sensor measurements," *IEEE/ASME Trans. Mechatronics*, vol. 19, no. 4, pp. 1343–1351, Aug. 2014.
[11] B. L. Anderson, J. G. Ho, W. D. Cowan, O. Blum-Spahn, A. Y. Yi, D. J. Rowe, M. R. Flannery, D. L. McCray, P. Chen, and D. J. Rabb, "Hardware demonstration of extremely compact optical true time delay device for wideband electronically steered antennas," *J. Lightw. Technol.*, vol. 29, no. 9, pp. 1343–1353, May 1, 2011.
[12] N. Le Chau, N. T. Tran, and T.-P. Dao, "A multi-response optimal design of bistable compliant mechanism using efficient approach of desirability, fuzzy logic, ANFIS and LAPO algorithm," *Appl. Soft Comput.*, vol. 94, Sep. 2020, Art. no. 106486.
[13] Y. Miao and J. Zheng, "Optimization design of compliant constant-force mechanism for apple picking actuator," *Comput. Electron. Agricult.*, vol. 170, Mar. 2020, Art. no. 105232.
[14] M. P. Dang, H. G. Le, N. Le Chau, and T.-P. Dao, "A multi-objective optimization design for a new linear compliant mechanism," *Optim. Eng.*, vol. 21, no. 2, pp. 673–705, Jun. 2020.

[15] N. L. Ho, T.-P. Dao, N. Le Chau, and S.-C. Huang, "Multi-objective optimization design of a compliant micrograpper based on hybrid teaching learning-based optimization algorithm," *Microsyst. Technol.*, vol. 25, no. 5, pp. 2067–2083, 2019.
[16] K. Noh, M. Zhang, and E. Sánchez-Sinencio, "A unified amplifier-based CC-CV linear charger for energy-constrained low-power applications," *IEEE Trans. Circuits Syst. II, Exp. Briefs*, vol. 66, no. 3, pp. 377–381, Mar. 2019.
[17] Y. Kaymak, R. Rojas-Cessa, J. Feng, N. Ansari, and M. Zhou, "On divergence-angle efficiency of a laser beam in free-space optical communications for high-speed trains," *IEEE Trans. Veh. Technol.*, vol. 66, no. 9, pp. 7677–7687, Sep. 2017.
[18] J. Fu, C. Yan, W. Liu, and T. Yuan, "Simplified equations of the compliant matrix for right elliptical flexure hinges," *Rev. Sci. Instrum.*, vol. 86, no. 11, Nov. 2015, Art. no. 115115, doi: 10.1063/1.4936212.
[19] A. Zhiwei, J. Jianbo, W. Pengjv, L. Jing, and Z. Haoyang, "Integrative design of structure control for two-axis fast steering mirror with flexible support," *Infr. Laser Eng.*, vol. 49, no. 7, pp. 235–242, Jul. 2020, doi: 10.3788/IRLA20190479.
[20] Y.-F. Lu, D.-P. Fan, Z.-Y. Zhang, and Q.-K. Zhou, "Design of two-axis elastic support for fast steering mirror," *Opt. Precis. Eng.*, vol. 18, no. 12, pp. 2574–2582, Dec. 2010, doi: 10.3788/OPE.20101812.2574.
[21] B. Ran, P. Yang, L. Wen, R. Du, K. Yang, S. Wang, and B. Xu, "Design and analysis of a reactionless large-aperture fast steering mirror with piezoelectric actuators," *Appl. Opt.*, vol. 59, pp. 1169–1179, Feb. 2020.
[22] N. Lobontiu, J. S. N. Paine, E. O'Malley, and M. Samuelson, "Parabolic and hyperbolic flexure hinges: Flexibility, motion precision and stress characterization based on compliance closed-form equations," *Precis. Eng.*, vol. 26, no. 2, pp. 183–192, Apr. 2002, doi: 10.1016/S0141-6359(01)00108-8.
[23] J. Yuan, X. Wang, C. Yan, S. Chen, S. Wang, J. Zhang, Z. Xu, X. Ju, N. Ding, Y. Dong, and W. Zhang, "Wavelength selection for estimating soil organic matter contents through the radiative transfer model," *IEEE Access*, vol. 8, pp. 176286–176293, 2020, doi: 10.1109/ACCESS.2020.3026813.
[24] X. Liu, J. Sun, L. Zheng, S. Wang, Y. Liu, and T. Wei, "Parallelization and optimization of NSGA-II on sunway TaihuLight system," *IEEE Trans. Parallel Distrib. Syst.*, vol. 32, no. 4, pp. 975–987, Apr. 2021, doi: 10.1109/TPDS.2020.3037082.
[25] J.-J. Fu, C.-X. Yan, W. Liu, and T. Yuan, "Stiffness calculation and optimal design of elliptical flexure hinges," *Opt. Precis. Eng.*, vol. 24, no. 7, pp. 1703–1710, 2016, doi: 10.3788/OPE.20162407.1703.

WEIFAN ZHANG was born in Chongqing, China, in 1996. He received the B.S. degree in agriculture science from Southwest University, China, in 2018. He is currently pursuing the M.S. degree in mechanical engineering with the Changchun Institute of Optics, Fine Mechanics and Physics, Chinese Academy of Sciences, Changchun, China. His current research interests include integrated design and optimization of optical machine structure and structural topology optimization design.

JING YUAN was born in Changchun, Jilin, China, in 1993. She received the B.S. degree in optical information science and technology from Jilin University, China, in 2016. She is currently pursuing the Ph.D. degree in optical engineering with the Changchun Institute of Optics, Fine Mechanics and Physics, Chinese Academy of Sciences, Changchun. Her current research interests include application of spectra, hyper-spectral remote sensing, and application of remote sensing in soil.

CHANGXIANG YAN was born in Honghu, Hubei, China, in 1973. He received the M.S. degree in engineering from Zhejiang University, Zhejiang, China, in 1998, and the Ph.D. degree from the Changchun Institute of Optics, Fine Mechanics and Physics, Chinese Academy of Sciences, Changchun, China, in 2001.

Since 2010, he has been the Director of the Space Optics Laboratory, Changchun Institute of Optics, Fine Mechanics and Physics, Chinese Academy of Sciences. His research interests include opto-mechatronics technology for space optical remote sensing instruments, multispectral and hyper-spectral spatial remote sensing imaging, polarization detection, and space surveillance.

ZHILIANG GAO was born in Gaomi, Shandong, China, in 1962. He received the B.S. degree in computer and application from the Night University of Changchun Institute of Optics and Fine Mechanics, Changchun, China, in 1995, and the M.S. degree from the Changchun University of Science and Technology, Changchun, in 2003.

He is currently a Senior Engineer and a Master Tutor. He is mainly involved in the design of spaceborne cameras, hyperspectral instruments, and related mechanical structures.

YOUZHI DONG was born in Harbin, Heilongjiang, China, in 1996. He received the B.S. degree in optoelectronic information science and engineering from Jilin University, China, in 2018. He is currently pursuing the M.S. degree in optical engineering with the Changchun Institute of Optics, Fine Mechanics and Physics, Chinese Academy of Sciences, Changchun, China. His current research interests include design of optical system of polarization spectral imager and large field of view lens.